HHS Public Access

Author manuscript

Langmuir. Author manuscript; available in PMC 2018 August 23.

Published in final edited form as:

Langmuir. 2018 July 31; 34(30): 8939–8951. doi:10.1021/acs.langmuir.8b01661.

Structure Dependence of Pyridine and Benzene Derivatives on Interactions with Model Membranes

Benjamin J. Peters[1], **Cameron Van Cleave**[1], **Allison A. Haase**[1], **John Peter B. Hough**[1,2], **Keisha A. Giffen-Kent**[1], **Gabriel M. Cardiff**[1,3], **Audra G. Sostarecz**[4], **Dean C. Crick**[5,6], and **Debbie C. Crans**[1,6]

[1]Department of Chemistry of Colorado State University, Fort Collins, Colorado, 80523, United States

[2]Department of Biochemistry Colorado State University, Fort Collins, Colorado, 80523, United States

[3]Department of Biology Colorado State University, Fort Collins, Colorado, 80523, United States

[4]Department of Chemistry Monmouth College, Monmouth, Illinois, 61462, United States

[5]Department of Microbiology, Immunology, and Pathology, Colorado State University, Fort Collins, Colorado, 80523, United States

[6]Cell and Molecular Biology Program Colorado State University, Fort Collins, Colorado, 80523, United States

Abstract

Pyridine based small molecule drugs, vitamins, and cofactors are vital for many cellular processes, but little is known about their interactions with membrane interfaces. These specific membrane interactions of these small molecules or ions can assist in diffusion across membranes or reach a membrane bound target This study explores how minor differences in small molecules (isoniazid, benzhydrazide, isonicotinamide, nicotinamide, picolinamide, and benzamide) can affect their interactions with model membranes. Langmuir monolayer studies of dipalmitoylphosphatidylcholine (DPPC) or dipalmitoylphosphatidylethanolamine (DPPE), in the presence of the molecules listed, show that isoniazid and isonicotinamide affect the DPPE monolayer at lower concentrations than the DPPC monolayer, demonstrating a preference for one phospholipid over the other. The Langmuir monolayer studies also suggest that nitrogen content and stereochemistry of the small molecule can affect the phospholipid monolayers differently. To determine the molecular interactions of the simple N-containing aromatic pyridines with a membrane-like interface, ^{1}H 1D NMR and ^{1}H-^{1}H 2D NMR techniques were utilized to obtain information aboutposition and orientation of the molecules of interest within aerosol-OT (AOT) reverse micelles. These studies show that all six of the molecules reside near the AOT sulfonate headgroups and ester linkages in similar positions, but nicotinamide and picolinamide tilt at the

Correspondence to: Debbie C. Crans.

Author Contributions

The manuscript was written through contributions of all authors. All authors have given approval to the final version of the manuscript.

The authors declare no competing financial interest.

water-AOT interface to varying degrees. Combined, these studies demonstrate that small structural changes of small N-containing molecules can affect their specific interactions with membrane-like interfaces, and specificity toward different membrane components.

Graphical Abstract

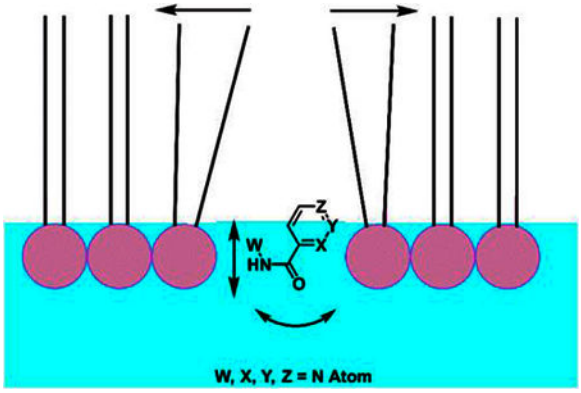

Keywords

Langmuir monolayer; reverse micelle; phospholipid; isoniazid; nicotinamide; pyridine; NMR spectroscopy; membrane

INTRODUCTION

Small molecules (<500 Daltons) have been the cornerstone for medical treatment, supplements, and preservatives, with many diffusing through the cellular membrane to reach their target.[1,5] One such example is a very successful first line anti-tuberculosis drug, isoniazid (INH, Figure 1), which has been shown to diffuse across the membrane of *Mycobacterium tuberculosis,* where INH is then able to reach the target, KatG.[67] Similar to INH, the method of entry into a cell for many small molecules has been studied in detail,[8,12] but there is a lack of information pertaining to the specific interactions of small molecules with the membrane interfaces. This lack of information is in large part due to the difficulty of determining the specific interactions of molecules with the lipids that make up the membranes, and the complexity of the biological membranes themselves.[13‘15] The specific small molecule-lipid interactions of a series of aromatic N-containing compounds were studied here (Figure1) to understand how small molecules are taken into cells, how they affect the membrane, and may elucidate aspects of the small molecule’s mode of action.

Many of these small molecules used to treat diseases such as tuberculosis, contain a pyridine as their main structural component[16,18] The presence and placement of nitrogen within the pyridine ring has great effects on these small molecules and their inter- and intramolecular interactions. For example, the amide group of picolinamide (PIC) is ortho to the pyridine nitrogen allowing for intramolecular hydrogen bonding (Figure 1).[19,20] This increases the molecule’s hydrophobicity and allows it to penetrate a membrane interface deep enough to affect the packing of the phospholipid tails.[21,22] This behavior is not observed for

nicotinamide (NIC, meta) nor isonicotinamide (iNIC, para) since the amide and pyridine nitrogen are not in proximity for intramolecular hydrogen bond formation.[19,20] Despite this difference, Olsson *et. al.* were able to show that NIC tightly binds to plasma membrane extracts of human leukemic K-562 cells (Kd between 3.2 and 12.7 μM).[9] Because such small differences in structure have such profound effects on inter-and intramolecular interactions, we hypothesize here that these molecules may interact with a membrane interface differently despite having similar structures as shown in Figure 1.

To study how small structural differences can affect interactions with membrane interfaces, this study aims to explore the interactions of the molecules in Figure 1 with two model membrane interfaces (Figure 2). The first model membrane, Langmuir monolayer, has been used to obtain free energies of mixing of hydrophobic molecules,[23–25] explore phenomena within the membrane,[26–28] and to test how molecules affect a lipid interface.[29–32] While compressing a phospholipid Langmuir monolayer in the presence of the molecules shown in Figure 1, it is possible to determine if the molecules expand, reorganize, or affect the compressibility of the phospholipid monolayer.[33] A commonly used phospholipid, dipalmitoylphosphatidylcholine (DPPC) can comprises up to 40% of lung phospholipid content because of its superior ability to expand and spread at the lung alveolar air-liquid interface.[34–36] Similarly, dipalmitoylphosphatidylethanolamine (DPPE) is utilized to model the inner leaflet of bacterial and eukaryotic membranes for drug and lipid interactions.[37–38] These two lipids have become a very appealing model interface to study drug and lipid interactions and therefore were used in this study as a model membrane interface to study the interactions of the N-containing compounds in Figure 1.[34–36,37–38] To determine the molecular-detail interactions of small aromatic N-containing compound with an interface, aerosol-OT (AOT) reverse micelles (RM) [39–42] were examined.[30. 43–47] RMs are self-assembled microemulsion that form at low water concentration. In these systems the placement and orientation could be identified by monitoring interactions with the AOT headgroup and/or lipid tails using ID and 2D NMR spectroscopic techniques.[3043–47] With the combination of these two model membrane systems (Figure 2), information about how the compounds in Figure 1 interact with membrane-like interfaces was obtained in this study.

MATERIALS AND METHODS

General Materials.

Most materials were used without further purification. Benzamide (BA) (99%), PIC (98%), NIC (98%), iNIC (99%), INH (≥99%), benzhydrazide (BHZ) (98%), isooctane (2,2,4 trimethylpentane, 99.8%), methanol (≥99.9%), activated charcoal (99.5%), chloroform (≥99.5%), deuterium oxide (99.9%), 2,2-dimethyl-2-si-lapentane-5-sulfonate sodium salt (DSS, 97%), monosodium phosphate (≥99.0%), disodium phosphate (≥99.0%), sodium hydroxide (≥98%), and hydrochloric acid (37%) were all purchased from Sigma-Aldrich. DPPC (≥99%) and DPPE (99%) were purchased from Avanti Polar Lipids. Sodium AOT (aerosol-OT, bis(2-ethylhexyl)sulfosuccinate sodium salt, ≥99.0%) was purchased from Sigma-Aldrich and was purified further as has been reported previously to remove any acidic impurities.[30] Briefly, 50.0 g AOT was dissolved into 150 mL of methanol to which 15 g

activated charcoal was added. This suspension was stirred for 2 weeks. After mixing, the suspension was filtered to remove the activated charcoal. The filtrate was then dried under rotary evaporation at 50 °C until the water content was below 0.2 molecules of water per AOT as determined by ^{1}H NMR spectroscopy. The pH was adjusted throughout this study using varying concentrations of NaOH or HC1 dissolved/mixed in either D_2O or H_2O depending on experimental requirements. NaOH or HC1 dissolved in D_2O is referred to as NaOD or DC1 respectively.

Preparation of Phospholipid Langmuir Monolayers.

Phospholipid stock solutions were prepared by dissolving DPPC (0.018 g, 0.025 mmol) or DPPE (0.017 g, 0.025 mmol) in 25 mL of 9:1 chloroforrmmethanol (v:v) for a final concentration of 1 mM phospholipid. The aqueous subphase consisted of 50 mL of 20 mM sodium phosphate buffer (pH 7.4) and varying concentrations of hydrazide of amide (10, 0.10, or 0 mM hydrazide or amide). Sodium phosphate buffer (20 mM, pH 7.4) instead of double deionized H_2O (DDI H_2O) was used as the subphase for the compression isotherms for better pH control (Figure S2).[30] Before addition of the phospholipid monolayers, the surface of the subphase was cleaned using vacuum aspiration and to make sure the surface was clean, the surface pressure of a compression isotherm of just the subphase (no phospholipid present) was measured (surface pressure was consist-entlyO.O +/− 0.5 mN/m throughout compression). To prepare the phospholipid monolayer, 20 μL of phospholipid stock solution (20 nmol of phospholipid, 112 A^2/molecule) was added to the surface of the subphase in a dropwise manner using a Hamilton syringe. The film was allowed to equilibrate for 15 minutes. The resulting phospholipid monolayer was then used for the compression isotherm experiments (see Figured 2A).

Compression isotherm surface pressure measurements of Langmuir monolayers.

The phospholipid mono-layer was compressed from 2 sides with a total speed of 10 mm/min (5 mm/min from opposite sides, Figure 2A) using a Kibron pTroughXS equipped with a Teflon ribbon (polytetrafluoroethylene, hydrophobic barrier). The temperature was maintained at 25 °C using an external water bath. The surface tension of the subphase during each compression was monitored using a wire probe as a Wilhemy plate. The surface pressure was calculated from the surface tension using equation 1 where $\boldsymbol{\pi}$ is the surface pressure, y_0 is the surface tension of water (72.8 mN/m), and $\boldsymbol{\gamma}$ is the surface tension at a given area per phospholipid after the film has been applied.

$$\pi = \gamma_o - \gamma \quad (1)$$

Each compression isotherm experiment consisted of at least 3 replicates and the averages with standard deviations of the area per phospholipid at every 5 mN/m was calculated using Microsoft Excel. The worked-up data were transferred to OriginPro Version 9.1 to be graphed. From the averages of the compression isotherms, the percent difference from the control of each sample at 5mN/m, 30 mN/m, and 35 mN/m were calculated. The compression moduli were calculated using OriginPro Version 9.1 from the compression

isotherm average results using equation 2, where Cs^1 is the compression modulus, A is the surface area, and π is the surface pressure.

$$C_s^{-1} = -A(dA / d\pi) \quad (2)$$

Preparation of RMs for Dynamic Light Scattering (DLS).

RMs were prepared as has previously been reported.[30] To prepare the 100 mM AOT stock solution, 2.2 g of purified AOT (4.9 mmol) was dissolved into 50 mL isooctane. The 10 mM aqueous stock solutions of amide orhydrazide were prepared by dissolving 50 μmol of amide or hydrazide into 5 mL DDI H_2O and then the pH was adjusted to pH 7.0. To prepare the RM solutions, specific volumes of the AOT stock solution and aqueous solution were added for a total of 5 mL to form RM sizes of w_0 8,12,16, and 20 where $w_0 = [H_2O]/[A0T]$, Upon mixingtheAOT stock solution with aqueous solution, a white aggregate formed at the water-isooctane interface. Then the mixture was vortexed until clear (—30 s), consistent with the formation of RMs.[30]

Parameters for DLS Analysis.

Once the glass cuvettes (1 cm × 1 cm) had been washed with isooctane and RM sample (3 times each), the cuvettes were filled with 1 ml of sample, and analyzed using a Zetasizer nano-ZS. The wavelength of light used was 632.8 nm and scattering was obtained at an angle of 173°. Each sample was equilibrated for 700 s at 25 °C then run for 10 scans per acquisition for 15 acquisitions. Each sample was run in triplicate, and the hydrodynamic radii (Rh) and polydispersity index (PDI) were averaged with the standard deviations reported in Table S1.

Preparation of Aqueous Stock Solutions of Amides and Hydrazides for RM Samples for ^{1}H NMR.

The aqueous stock solutions were prepared by dissolving 0.25 mmol (0.50 mmol for NIC) of amide or hydrazide into 25 mL of D_2O for a final concentration of 10 mM (20 mM for NIC). The NIC concentration was increased to obtain a greater signal to noise ratio in the ^{1}H NMR spectra of the RMs. Each aqueous stock solution was then pipetted into 2 mL aliquots and the pD (pD = pH + 0.4)[30–46] of each aliquot was adjusted using NaOD or DC1 solutions (5.0,1.0, and 0.1 M). The pD will be referred to as pH for the rest of this manuscript as is commonly done.[30–46] The pD of the aliquots was adjusted to a range between 1.2 and 9.0 for later use in determination the pKa in D_2O and in the w_0 16 RMs.

Preparation of AOT-Isooctane stock solution and RMs for ^{1}H NMR.

The 750 mM AOT stock solution was prepared by dissolving 8.34 g AOT (18.8 mmol) in 25 mL isooctane. This mixture was sonicated and vortexed until clear (approximately 15 min). Once dissolved, the solution was equilibrated to ambient room temperature. RMs of w_0 values of 8, 12, 16, and 20 were prepared by adding specific volumes of the stock AOT solution and the pH 7.0 aqueous aliquot 215 μL of the other aqueous aliquots of pH's

ranging from 1.2 to 9.0 and 785 μL of the AOT stock solution were mixed to form w_0 16 RMs at varying pH values. The indicated pH values of the RMs are assumed to be the same from the measured aqueous samples. All the RM mixtures were vortexed until clear as was done for DLS experiments.

^{1}H NMR of D_2O and RM Samples.

The ^{1}H NMR experiments were performed using a 400 MHz Varian NMR spectrometer using standard parameters (1s relaxation time, 25 °C, and 45° pulse angle). The aqueous samples were referenced to an external DSS sample at pH values of 1.2,1.5,2.0, 2.5, and 3.0. Above pH 3.0 the DSS methyl silane peak was consistent and therefore the pH 3 DSS standard was used as the standard for the aqueous samples at higher pH values. RM samples were referenced to the isooctane methyl peak at 0.90 ppm as has been previously reported and was originally referenced to tetramethyl silane (TMS).[30,43,46] The resulting spectra were analyzed using MestReNova Version 10.0.1. The pKa values were determined by plotting the chemical shifts of the samples at different pH values in D_2O and in w_0 16 RMs and then taking the first derivative of the best fit curve using OriginPro Version 9.1 (see Figure S3).[30]

Preparation of RMs for ^{1}H-^{1}H 2D NOESY and ROESY NMR.

The 750 mM AOT stock solution was prepared by dissolving 0.34 g AOT (0.76 mmol) in 1 mL of isooctane. To form the RM (wo 12), 839 pL of AOT stock solution was added to 161 pL of D_2O and vortexed until clear. This suspension was then mixed with 32 pmol of amide or hydrazide for an average concentration of 200 mM amide or hydrazide within the RM water pool (32.2 mM overall). The mixture was vortexed until the solid dissolved into the RM microemulsion.

Parameters for Recording the ^{1}H-^{1}H 2D NOESY and ROESY NMR Spectra.

The ^{1}H-^{1}H 2D NOESY and ROESY experiments were conducted using a 400 MHz Varian NMR at 26 °C with 16 scans per transient and 256 transient pairs in the fl dimension. The ^{1}H-^{1}H 2D NOESY spectrum was acquired using a standard pulse sequence with a mixing time of 200 ms and a 1.5 s relaxation delay. The ^{1}H-^{1}H 2D ROESY spectra were acquired using a standard pulse sequence with a 200,100, or 0 ms mixing time and a 1.5 s relaxation delay. The resulting spectra were analyzed using Mestrenova Version 10.0.1 by subjecting the spectra to a 90° sine^2 weighting function with a first point at 0.50. The spectra were then phased and baselined using a third order Bernstein polynomial baseline. Each spectrum was referenced to the isooctane methyl peak at 0.904 ppm in both dimensions.[30]

RESULTS AND DISCUSSION

Interactions of Aromatic Hydrazides with Langmuir Monolayers.

Surface pressure compression isotherms of DPPC and DPPE were measured to model phospholipids commonly found in eukaryotic and bacterial membranes.[34–38] The minor structural difference in the lipid headgroup results in significant differences in the properties of the resulting lipid monolayer. DPPE has a conical shape and packs much more tightly compared to DPPC which has a cylindrical shape. This is thought to be due to the hydrogen bonding capability of DPPE (ethanolamine head group) that DPPC (choline headgroup) is

lacking.[48–49] For these reasons, both DPPC and DPPE zwitterionic phospholipids were used to form Langmuir monolayers to study the interactions of small molecules with phospholipid interfaces.

Surface pressure compression isotherms of DPPC or DPPE were initially conducted in the presence of INH or BHZ hydrazides (Figure 3A-D). The area per phospholipid of the DPPC monolayer in the presence of 10 mM INH increased, until 20–25 mN/m. The area per phospholipid of the DPPE monolayer in the presence of all concentrations of INH tested increased until 25–30 mN/m. In the presence of 10 mM BHZ, the area per phospholipid of the DPPC monolayer increased until 15–20 mN/m and the area per phospholipid of the DPPE monolayer was unaffected. Briefly, INH affected the area per phospholipid of both monolayers but at all concentrations only for the DPPE monolayer, while BHZ only affected the area per phospholipid of the DPPC monolayer.

To determine if the compressibility of the monolayers was affected, the compression modulus was calculated from the average compression isotherms (Figure S6). In the presence of 10 mM INH, the compression modulus of the DPPC monolayer decreased and all concentrations of INH tested, caused a decrease in the compression modulus of the DPPE monolayer. The presence of 10 mM BHZ decreased the compression modulus of the DPPC monolayer and increased the compression modulus in the presence of 10 mM BHZ. All concentrations tested of BHZ present increased the compression modulus of the DPPE monolayer. In summary, INH decreased the compression modulus of both DPPC and DPPE monolayers, but only the DPPE monolayer was affected at all concentrations tested. BHZ decreased the compression modulus of the DPPC monolayer and with 1 mM BHZ present; the compression modulus of the DPPE monolayer increased.

Generally, an increase in area per phospholipid of a monolayer indicates an uptake of the small molecule causing the monolayer to spread, and a decrease in area per phospholipid indicates either solubilization of lipid or a reorganization to allow for tighter packing of the phospholipid monolayer. A decrease in compression modulus has been commonly interpreted as an increase in compressibility and vice versa.[29,50] INH did increase the area per phospholipid of both the DPPC and DPPE monolayers indicating an uptake into the phospholipid monolayers, but did so at lower concentrations present for DPPE. A similar trend was observed with the decrease of compression moduli in the presence of INH. This suggests that INH has a higher affinity for DPPE than DPPC, indicating that INH would interact more favorably with the ethanolamine than the choline head group. This is presumably due to hydrogen bonding with the ethanolamine head group which would disrupt the intermolecular hydrogen bonding between individual DPPE molecules of the DPPE monolayer.[48,49] BHZ affected the area per phospholipid of only the DPPC monolayer at 10 mM and decreased the compression modulus suggesting that at high concentration, BHZ is taken into and allows for easier compression of the DPPC monolayer. At 1 mM for DPPC and all concentrations tested for DPPE; BHZ does not affect the area per phospholipid but increases the compression modulus showing that the BHZ did not spread the phospholipids, but did cause the monolayer to be more difficult to compress than the control monolayers. This suggests that BHZ is reorganizing the phospholipid tails, but more information would be needed for confirmation. In summary, INH was shown to prefer the

ethanolamine head group and allowed for easier compression than the control phospholipid monolayers, while BHZ allowed for easier compression and spread the DPPC monolayer when 10 mM was present in the subphase, but otherwise caused the phospholipid monolayers to be less compressible without affecting the area per phospholipid.

Interactions of Aromatic Amides with Langmuir Monolayers.

To determine if the amides in Figure 1 interact with phospholipid interfaces differently, the surface pressure compression isotherms of DPPC and DPPE were conducted in the presence of BA, PIC, NIC, and iNIC, shown in Figure 4 and compression moduli are given in Figure S11.

First, the compression isotherm experiments using BA were conducted as a nitrogen deficient comparison. The presence of 10 mM BA, the DPPC monolayer exhibited an increase in pressure below 15–20 mN/m and then above 15–20 mN/m, exhibited a slight decrease in area per phospholipid. The DPPE monolayer increased in area per phospholipid until 15–20 mN/m. The compression modulus (Figure S11) of the DPPC monolayer decreased in the presence of 10 mM and 0.1 mM BA and increased when 1.0 mM was present. Concentrations of 10 mM and 0.1 mM BA also decreased the compression modulus of the DPPE monolayer. This data suggests that BA can spread the phospholipids of both DPPC and DPPE until higher pressures, but it can still affect the compressibility of the phospholipid monolayers showing that BA still does interact with the monolayer at higher pressures.

In the presence of 10 mM PIC, the DPPC and DPPE monolayers exhibited an increase in area per phospholipid as compared to the control monolayers until 35–40 mN/m. Also, depending on the concentration of PIC within the subphase, the compression modulus either decreased for DPPC (10 mM), increased (1 mM), or no effect was observed (0.1 mM). The DPPE monolayer compression modulus was increased only by the presence of the 0.10 mM PIC. The increase in area per phospholipid of DPPC and DPPE in the presence of PIC suggests that PIC is spreading the lipids; but depending on the concentrations of PIC, the compressibility of the phospholipid monolayers is affected (Figure S11). The dependence of the compressibility on the concentration may be due to counteracting effects where a large amount of PIC (10 mM) increases compressibility solely because PIC exists in excess within the monolayer, so it is compressed out of the monolayer. At lower concentrations (1 mM for DPPC and 0.10 mM for DPPE), PIC caused the monolayers to become more rigid and less compressible. Briefly, PIC did increase the area per phospholipid of both phospholipid monolayers, and had varying effects on the compression moduli of the phospholipid monolayers.

The DPPC and DPPE monolayers in the presence of NIC both exhibited an increase in area per phospholipid. All concentrations of NIC tested increased the area per phospholipid of DPPC above 10 mN/m. The DPPE monolayer was affected in a concentration dependent manner where 10 mM NIC increased the are per molecule the most. The presence of 10 mM NIC caused an increase in area per phospholipid of DPPE across at all surface pressures below collapse (55mN/m). There was not much of an effect of NIC on the compression modulus on the DPPC monolayer (Figure S11); however, there was a decrease in the

compression modulus for the DPPE monolayer at all concentrations of NIC tested. The presence of NIC caused a spreading of both phospholipid monolayers but only affected the compressibility of the DPPE monolayer allowing itto become more compressible than the control monolayer.

Unlike the other molecules tested, iNIC had no effect on either the DPPC nor the DPPE monolayer area per phospholipid. The presence of 10 and 1.0 mM iNIC did however decrease the compression modulus of the DPPE monolayer but did not have much of an effect on the compressibility of the DPPC monolayer (Figure Sll). This suggests that iNIC has a higher affinity for DPPE than DPPC and allows the DPPE monolayer to be more easily compressed without spreading the phospholipids.

By comparing the interactions of all the molecules of interest with DPPC and DPPE monolayers, it is clear that not all of the aromatic N-substituted compounds interact with the phospholipid monolayers in the same manner (Figure 4, Table 1). Out of the six compounds tested, INH and iNIC exhibited more of an effect on the DPPE monolayer than the DPPC monolayer suggesting a preference for the ethanolamine head group more so than the choline head group. This is most likely due to the ethanolamine's greater hydrogen bonding capacity than choline, allowing for intermolecular interaction. When comparing PIC, NIC, and the iNIC, the data is consistent with PIC and NIC affecting the phospholipid monolayers similarly, but iNIC had the least effect on the phospholipid monolayers. As shown in Table 1, NIC and PIC were the only compounds to significantly increase the area per phospholipid of the DPPC and DPPE monolayers at physiologically relevant surface pressures (30–35 mN/m),[51] whereas iNIC did not have much of an effect on the area per phospholipid. Of all the compounds, BA was the only molecule to cause a decrease in area per phospholipid for DPPC at higher surface pressures (above 15–20 mN/m, Table 1) suggesting that BA was the only compound tested that either reorganized DPPC to condense further or assist in the solvation of the DPPC. Interestingly, BHZ did not have the same effect as BA, but still interacted with the phospholipid monolayers causing the phospholipids to spread. In summary, INH and iNIC both exhibited a preference for DPPE over DPPC, PIC and NIC affect the phospholipid monolayers similarly even at high pressures, BA reorganizes the DPPC monolayer or helps solubilize the DPPC, and BHZ does interact with both monolayers causing spreading of the phospholipids.

Placement of Small Aromatic Hydrazides and Amides Within the AOT RM.

Molecular information on the specific interaction and placement of the compounds with respect to a membrane interface was sought using AOT RMs and NMR spectroscopy.[30,43–47,52] To this end, the ^{1}H NMR spectrum of each N-containing compound was acquired in D_2O and varying sizes of RM. By varying the sizes of the RM (wo), small changes in the RM microenvironment occur. Comparing the chemical shifts of the N-containing compounds caused by varying environmental differences, it is possible to place the compounds within the RM.[30,43–47,52] The following paragraphs describe the chemical shifting and our placement of compounds as a result of the observed chemical shifting patterns.

The ^{1}H NMR spectra of INH and iNIC are presented as stack plots of ^{1}H NMR spectra in D_2O at the bottom and the RM microemulsions with the smallest RMs as the top spectrum ($w_0$8, Figure 5). In the INH spectra, the H_a doublet peak shifts slightly downfield from the D_2O spectrum at 8.67 to 8.71 ppm in the $w_0$20 spectrum and then gradually shifts upfield to 8.70 ppm in $w_0$8 spectrum. The doublet Hb peak for INH shifted gradually downfield from 7.69 ppm in D_2O to 7.80 ppm in the W08 spectrum. A similar shifting pattern was observed with iNIC. The peak corresponding to the doublet H_a for iNIC barely shifts from 8.70 ppm in D_2O to 8.74 ppm in the $w_0$20 spectrum and then a slight upfield shift to the $w_0$8 spectrum at 8.72 ppm. The doublet peak corresponding to Hb shifts gradually downfield from 7.76 ppm in the D_2O spectrum to 7.86 ppm in the $w_0$8 spectrum. The downfield shifting of both H_a and Hb peaks of INH and iNIC from the D_2O spectrum to the $w_0$20 spectrum is consistentwith a more charged (deshielded) environment such as near the sulfonates of the AOT.[53] The upfield shifting pattern of H_a of both compounds is consistent with the reduction of a charged environment as the RM sizes are reduced suggesting that H_a is more toward the hydrophobic region than Hb.[53] Together this data suggests that both INH and iNIC reside near the AOT headgroups with the pyridine nitrogen facing toward the AOT tails and the amide/hydrazide toward the water pool similar to benzoate and phenyl biguanide.[30,46]

Next, the interactions of the benzene based hydrazide and amide, BHZ and BA, with the AOT RM interface are described by ^{1}H NMR. The doublet corresponding to H_a for BHZ shifted from 7.74 ppm in the D_2O spectrum to 7.94 ppm gradually as the RM sizes were reduced to the $w_0$8 spectrum. The triplets corresponding to Hb and H_c for BHZ are at 7.62 ppm and 7.52 ppm respectively in the D_2O spectrum and then coalesce in the RM spectra while gradually shifting upfield to 7.38 ppm in the $w_0$8 spectrum. The peak corresponding to H_a for BA shifts from 7.83 ppm in D_2O gradually to 7.99 ppm in the $w_0$8 spectrum. The peaks corresponding to Hb and H_c of BA in the D_2O spectrum are at 7.64 ppm and 7.53 ppm respectively and then coalesce in the RM spectra and gradually shift upfield until 7.40 ppm in the $w_0$8 spectrum. The downfield shifting pattern of H_a of both BHZ and BA from D_2O spectrum to the $w_0$8 spectrum is consistent with the RM interface. The upfield shifting pattern of Hb and He of both BHZ and BA is consistent with a deep placement within the RM interface toward the AOT tails. Using this data, it is possible to place BHZ and BA within the water-AOT interface with the benzene ring of both compounds placed a little more toward the AOT tails than INH and iNIC, and with the amide/hydrazide toward the water pool. This is similar to what has been previously found for benzoic acid.[30]

The position and orientation of NIC within the RM was explored by itself unlike the previous compounds. The doublet corresponding to H_a for NIC shifted gradually downfield from 8.94 ppm in the D_2O spectrum to 9.10 ppm in the $w_0$8 spectrum. The Hb doublet shifts from 8.72 ppm in the D_2O spectrum to 8.74 ppm in the $w_0$20 spectrum, and then shifts upfield to 8.71 ppm in the $w_0$8 spectrum. The H_c doublet shifts from 8.27 ppm in the D_2O spectrum gradually to 8.34 ppm in the $w_0$8 spectrum, and the Hd peak is the only peak for NIC to gradually shift upfield from 7.62 ppm in the D_2O spectrum to 7.52 ppm in the w_0 8 spectrum. The downfield shifting for the Hd and H_a peaks for NIC are consistent with placement toward the water-AOT interface. The H_c peak initially shifted downfield and then slightly upfield suggesting a placement near the water-AOT interface but more toward the

AOT tails than Hd and H_a. The Hb peak was the only peak that consistently shifted upfield suggesting the deepest placement (toward AOT tails) of all the NIC protons. This data is consistent with NIC residing near the water-AOT interface with NIC tilted at the interface. This position would have H_a pointing toward the water pool and the amide tilted more toward the AOT headgroups. A similar finding was determined for the ortho-fluorobenzoate anion at the micellar interface.[53]

Finally, the placement and orientation of PIC within the RM samples was determined. The H_a doublet for PIC shifts slightly upfield from the 8.63 ppm in the D_2O spectrum to 8.60 ppm in the w_0 8 spectrum. The peaks corresponding to Hb and H_c are overlapping in the D_2O spectrum but then separate within the RM samples with Hb shifting downfield gradually from 8.04 ppm in the D_2O spectrum to 8.24 ppm in the w_0 8 spectrum and H_c gradually shifts upfield from 8.02 ppm in the D_2O spectrum to 7.98 ppm in in the w_0 8 spectrum. The H_d peak for PIC gradually shifts upfield from 7.64 ppm in the D_2O spectrum to 7.45 ppm in the w_0 8 spectrum. The upfield shifting pattern of Ha, Hc, and Hd peaks is consistent with the protons being placed toward the AOT tails. The downfield shifting pattern of Hb is consistent with it being placed more toward the AOT interface. This data is consistent with PIC residing near the AOT head-groups, with only H_b being near the AOT headgroups and the other protons toward the AOT tails causing a tilt of the molecule within the interface.

In summary, this data shows that these N-containing molecules interact differently with the AOT RM, but reside at similar positions within the water-AOT interface. INH and iNIC were shown to reside within the AOT interface with the pyridine nitrogen facing toward the AOT tails and the hydrazide/amide toward the AOT head groups. BHZ and BA were shown to reside deeper toward the AOT tails than INH or iNIC but with the same orientation. PIC was shown to reside at the AOT interface as INH and iNIC, but slightly tilted at the interface with the nitrogen of the pyridine and the amide facing toward the AOT head group and water pool. NIC was also shown to be tilted with the proton between the amide and pyridine nitrogen facing the water pool. Generally, each molecule resided in similar positions, but the pyridine nitrogen to amide orientation did affected the overall molecular orientation at the water-AOT RM interface. This finding is similar to what has been shown for fluorobenzoate derivatives with micelles.[53]

^{1}H-^{1}H 2D NMR of Hydrazides and Amides Within the AOT RM Interface.

More information was sought to confirm the placement and orientation based on ^{1}H 1D NMR experiments, therefore through space ^{1}H-^{1}H 2D NOESY and ROESY experiments were conducted.[30, 43–45] Both ^{1}H-^{1}H 2D NOESY and ROESY spectra with a 200 ms mixing time and higher concentration of BA was acquired to explore which experiment would provide the best signal to noise ratio (Figure S13). With the ROESY data producing a better signal to noise ratio than the NOESY for these samples, other ROESY spectra were sought using 100 or 0 ms mixing times. The 0 ms mixing time serves as a negative control to confirm no magnetization transfer was observed between magnetically different protons.

A portion of the ^{1}H-^{1}H 2D ROESY NMR spectra for INH and iNIC within w_0 12 RMs are shown in Figure 6. The spectra of INH within the w_0 12 RM microemulsion show a diagonal

with two, negative, blue peaks corresponding to the Ha and Hb peaks of INH at 7.71 ppm and 7.77 ppm respectively. The positive, red, off diagonal cross peaks corresponding to Ha and Hb are observed in the spectra of 200 and 100 ms mixing time whereas no cross peaks were observed in the 0 ms mixing time spectrum as would be expected. In the 200 ms mixing time spectrum for INH, an off diagonal cross peak corresponding to Hb on INH and the methyl peak of either AOT or isooctane at 0.90 ppm on the f2 axis. In the 100 ms mixing time spectrum, off diagonal cross peaks for both Ha and Hb at 0.90 ppm on the f2 axis were observed and correspond to the AOT or isooctane methyl peak. Considering that the previous ^{1}H 1D NMR experiments have shown that INH and iNIC reside within the water-AOT interface, INH is most likely residing near the AOT ethyl CH3 protons with the CH3 protons tilted toward the interface (see Figure S12 for AOT assignments).

The spectra of the w_0 12 RM microemulsion with iNIC also indicated an interaction with the AOT interface similar to INH. Along the diagonal shown in Figure 6, two, negative, blue peaks corresponding to iNIC protons Ha and Hb at 8.70 ppm and 7.80 ppm respectively. Positive, red, off diagonal cross peaks between Ha and Hb in the 200 and 100 ms mixing time spectra are observed. Finally, no cross peaks were observed in the 0 ms mixing time spectrum. In the 200 ms mixing time spectrum, positive, red, off diagonal cross peaks with H_a and Hb of iNIC are observed at 1.30 ppm and 0.90 ppm on the f2 axis corresponding to the AOT CH2 and an isooctane or AOT CH3 peak, respectively. These peaks were not observed in either the 100 ms nor 0 ms mixing time spectra. Due to iNIC's insolubility in isooctane and its similar placement determined by the ^{1}H ID NMR studies, these results support the interpretation that iNIC interacts within the RM water-AOT resides at the interface near the sulfonate headgroups of the AOT similar to the vanadium dipicolinate complex.[54]

The ^{1}H-^{1}H 2D ROESY spectra of RMs containing BHZ and BA (Figure S14) were very similar. In the following these compounds will be discussed concurrently. As can be seen on the diagonal of the spectra of BHZ, there are two negative, blue peaks at 7.97 ppm and 7.43 ppm corresponding to H_a and Hb/H_c respectively. Within the 200 and 100 ms mixing time spectra, positive, red, off diagonal cross peaks are observed between the H_a and Hb/H_c peaks whereas no cross peaks are observed for the 0 ms mixing time spectrum. In the 200 ms mixing time spectrum positive, red, off diagonal cross peaks at 1.30 ppm and 0.90 ppm on the fl axis corresponding to the AOT CH2 peak, the AOT CH3, or isooctane CH3 peak and H_a and Hb/H_c can be observed. In the spectrum using 100 ms mixing time the same off diagonal peaks are observed except for the off diagonal cross peak at 1.30 ppm on the fl axis and 7.97 ppm on the f2 axis corresponding to the AOT CH2 and the H_a protons respectively. These cross peaks were also observed for BA where the only differences in the spectra were from the placement of the BA negative, blue peaks on the diagonal at 7.92 ppm for H_a and 7.39 ppm for Hb/H_c. This data suggests that BHZ and BA are both positioned nearby the AOT ethyl with the hydrazide/amide facing the water pool consistent with the ^{1}H ID NMR studies.

The ^{1}H-^{1}H 2D ROESY spectra of PIC, within RMs were acquired to confirm placement and orientation within the RM water-AOT interface. Figure S15 shows the ^{1}H-^{1}H 2D ROESY NMR spectra of PIC within w_0 12 RM microemulsion acquired using 200,100, and 0 ms

mixing times. Observed in each of these spectra are negative, blue peaks along the diagonal corresponding to H_a (8.60 ppm), Hb (8.19 ppm), H_c (7.99 ppm), and Hd (7.47 ppm). In the spectra acquired using 200 and 100 ms mixing times, there are positive, red, off diagonal cross peaks between the peaks corresponding to the PIC peaks whereas no off diagonal cross peaks are observed in the spectrum acquired using a 0 ms mixing time. In the 200 ms mixing time spectrum, positive, red, off diagonal cross peaks at 0.90 in the fl dimension corresponding to all the PIC peaks observed. The same positive, red, off diagonal cross peaks are observed using 100 ms mixing time with the exception of the off diagonal cross peak at 0.90 ppm in the fl dimension and 7.99 ppm in the f2 dimension corresponding to H_c of PIC. This confirms that PIC resides within the AOT interface and does interact with the CH3 of the ethyl of AOT.

The placement and orientation within RMs of NIC was explored using ^{1}H-^{1}H 2D ROESY NMR in the w_0 12 RM spectra shown in Figure S15. The peaks on the diagonal are negative, blue peaks corresponding to H_a (9.02 ppm), Hb (8.68 ppm), He (8.29 ppm), and Hd (7.50 ppm). Positive, red, off diagonal cross peaks between the NIC aromatic protons can be observed in the spectra acquired using 200 ms and 100 ms mixing times but not for the 0 ms mixing time spectrum. Positive, red, off diagonal cross peaks corresponding to AOT peaks can be observed at 0.90 ppm in the fl dimension and at 9.02 ppm, 8.68 ppm, 8.29 ppm, and 7.50 ppm in the f2 dimension. These peaks suggest that all the aromatic protons of NIC reside near a methyl. Three other positive, red, off diagonal cross peaks can be observed at 1.30 ppm in the fl dimension and at 8.68 ppm, 8.29 ppm, and 7.50 ppm in the f2 dimension corresponding to the Ch_2 AOT peak and Hb, H_c, and H_d. This data is consistent with NIC residing at the same position within the RM interface as the other probe molecules but H_a is notin proximity to the CH2 of the AOT ethyl. By rotating the C-C bonds of the ethyl of AOT, the CH3 of the ethyl can reach further than the CH2 suggesting that H_a is in a position away from the CH2. This would suggest a tilt in the NIC at the water-AOT interface supporting the interpretation of the ^{X}H ID NMR spectra.

In summary, the ^{1}H-^{1}H 2D ROESY NMR spectra of w_0 12 RMs containing the compounds of interest did support the results from the ^{1}H ID NMR spectra. The placement of each of these molecules using data from both the ID and 2D NMR experiments is illustrated in Figure 7. First of which, INH and iNIC both can be positioned near the AOT ethyl. Since iNIC exhibited interactions with the CH2 of the ethyl of AOT, iNIC is placed slightly deeper toward the tails of the AOT than INH. BHZ and BA both can be placed at the same position and slightly deeper than iNIC. The 2D NMR of PIC confirmed that it does reside within the interface of the water pool and AOT while the ID NMR suggested a tilt at the water-AOT interface. Briefly, all the molecules resided near the water-AOT interface however, PIC and NIC exhibited a tilted orientation within the interface (see Figure 7).

pK_a Measurement of the Hydrazides and Amides Within the AOT RM.

To explore how the AOT interface affects the aromatic N-containing molecules, the pKa values of the small aromatic molecules were determined. The pH within the RM water pool is not just simply the-log[H^+] as is normally used in the United States to calculate pKa in aqueous solutions.[55] The pH value within the RM water pool is much more complicated.

Depending on the charge of the head group surfactant used to form the RM microemulsion, a proton gradient can form.[56–57] The AOT RMs used in this study have a negative charge and therefore can cause an increase in proton concentration atthe interface.[55] The pKa of molecules have also been known to change within varying environments, such as the difference in pK_a values of a specific amino acid depends on whether or notit is in the center or on surface of a protein, therefore the RM may affect the small aromatic molecules' pKa value.[58]

The pK_a values of the aromatic N-containing molecules in D_2O and in w_0 16 RMs are shown and compared to literature and calculated values in Table 2.[59] The pIC, for BA was not determined in this study, because of BA's low pKa value. The pK_a of each of the probe molecules in D_2O are all very similar to both the predicted pK_a values and the experimentally determined pIC, values.[59] The small differences between the pK_a values found in this study and the experimental studies in aqueous solutions is most likely caused by differences in ionic strength, temperature, and differences caused by H_2O (reported pIC, values) or D_2O (this study). Within the RMs, the pK_a of each molecule lowered beyond measurement. This would support an interaction with the AOT itself or an effect of the high ionic strength of the interface.[30,39–40.55] Either possibility supports that the molecules reside within the RM interface.

DLS of RMs Containing Aromatic Hydrazides and Am-ides.

DLS was used to determine that RMs formed. In addition to confirming that the RMs form, we also demonstrated that the sizes of the systems measured were consistent with that reported in the literature (Table S1).[41] Furthermore, the measurements were done to investigate whether the addition of the compound alter the overall structure of the RMs studied. As shown in Table S1 no differences in sizes of RMs with and without the aromatic hydrazides and aromatic amides were observed.[41]

Evaluation and Implication of Findings in studies of Langmuir Monolayer and interfaces in AOT/isooctane RMs.

Studies in model systems are done to obtain information that may not be accessible in studies of the biological membranes. The two model systems used in the studies here both have advantages and limitations. Regardless, it is important to note that there are substantial differences between the AOT interface and a phospholipid interface. The differences in structure, curvature, surfactant/lipid density, and head group charge (negative vs. zwitterionic respectively), may impact the interactions of the molecules under investigation with regard to their interaction with interfaces.[14. 39–40.51] Although these differences exist, there are similarities between how the molecules of interest interact with the AOT interface and the phospholipid interface. By comparing the findings of the RM experiments with phospholipid Langmuir monolayer experiments, the combination can shed light on crucial differences behind the interactions of molecules with the surfactant or lipid interfaces.[30.45]

Interestingly, all the molecules studied here were found to reside near the head group of the AOT surfactant interface. The RM studies provide information about how small structural changes in the aromatic amide or hydrazide can affect compound placement and orientation

at a surfactant interface. This finding, albeit on a different type of interface, is consistent with the results reported in computational studies of NIC and PIC with phosphatidylcholine and phosphatidylethanolamine phospholipids[21–22] along with experimental studies with INH interacting with a liposome consisting of phosphotidylcholine.[60–61] We found that the distance of amide to the pyridine nitrogen and the molecular orientation of the amide can impact the interactions with the water-AOT interface. Similarly using computational methods in studies by Borba *et al.* and Martini *et al.* specific hydrogen bonding with NIC and PIC were found using phosphatidylcholine and phosphatidylethanolamine phospholipids.[21–22] Although the findings in our studies with the RMs do not directly demonstrate the specific interactions with the phospholipid headgroups found in these computational studies, but the locations identified in our studies of the small aromatics N-containing molecules with the sulfonate head group of AOT were comparable, that is placing the drug near the interface.

Conversely if the small aromatic N-containing compounds interacted primarily with the phospholipid tails, then the head group would not have affected the overall interactions with the phospholipids and the area per phospholipid would have been affected similarly between DPPC and DPPE. Since this was shown to not be the case in the Langmuir monolayer studies, the molecules of interest most likely also reside near the phospholipid head groups as found in the AOT RM experiments. The difference in interaction with DPPC vs. DPPE was especially evident with INH and iNIC (see Figure 3A–3B). The previous study by Marques *et al.* was able to determine a dissociation constant (Kd) of INH with dimyristoylphosphatidylcholine (DMPC) supported bilayers to be 0.031 μmol by plasmon waveguide resonance.[60,62] With the observation that INH most likely prefers DPPE to DPPC, the Kd of INH with DPPE would most likely be lower than that found by Marques *et al.* More studies are needed to determine the exact values and whether the difference in tail length would affect the Kd.

The Langmuir monolayer studies also support the interpretation that the orientation of the amide to pyridine nitrogen affect the phospholipid interface. This result was apparent from the differences in compression isotherm area per phospholipid caused by the presence of iNIC compared to NIC and PIC. NIC and PIC affected the monolayers similarly, in contrast to iNIC that affected the monolayers differently. INIC was more similar to INH where it preferred DPPE, but iNIC did not spread the lipids like NIC and PIC did. The similar overall effects on the phospholipid monolayers by PIC and NIC were most likely caused by different molecular interactions that happen to have similar outcomes as supported by a difference in tilting at the RM interface. To summarize, the specific structural characteristics of these compounds can influence their interactions with phospholipid and surfactant interfaces in a comparable manner.

When combining the information from these two model membrane systems, a few conclusions about the placement and interactions of the molecules of interest with surfactant and phospholipid interfaces can be made. The RM experiments show that despite a similar placement of all the molecules of interest within the water-AOT interface, the orientation of the pyridine nitrogen to the amide can affect the specific orientation of the whole molecule of interest within an interface. This tilt of PIC and NIC suggests that within other interfaces,

such as a phospholipid interface, the small difference between these molecules can allow for differences in the interactions with a phospholipid monolayer. Although, those interactions will likely not be the same as determined from the RM experiments.[21] The phospholipid Langmuir monolayer studies build on this idea by also supporting the expectation that the specifics behind the interactions of the head group of the phospholipid with the molecule of interest can affect binding such as what was observed with INH and iNIC. To summarize, the hypothesis that small differences in structure can lead to differences in the interactions of these small molecules with membrane interfaces, was supported by these observations.

Although this study focused exclusively on monolayers, the observations gathered can cautiouslybe used to provide some projections about how these molecules might pass through a bilayer membrane. With each molecule studied here, they all resided within the water-AOT RM interface and interacted differently with phospholipids containing the same tail but different head groups. Together, these observations would support a head group based interaction of the drugs in contrast to interactions with the choline, phosphate, or glycerol of phospholipids. Therefore these compounds may not passively diffuse through a bilayer membrane like weak acid preservatives (ex. benzoic acid and fomic acid) or protonophores (ex. carbonyl cyanide m-chlorophenyl hydrazine).[8,10,30] If the molecules are able to traverse a membrane by passive diffusion, then it would be expected that the molecules would reside deeper within the RM tails/organic solvent.[30] The data obtained in this study does not support passive transport of these small aromatic N-containing compounds.

Other methods for crossing a bilayer has been extensively studied using different cations and anions. In these method, cations or anions are transported through forming a complex with phospholipids and then flip with the phospholipid across the bilayer, or through a hydrophobic pore that may form allowing traversing of ions.[63–67] Some of these mechanisms have been studied through computational studies, and Borba *et al.* was able to show that the binding of PIC and NIC to the phosphatidylcholine or phosphatidylethanolamine head groups can cause conformational differences in the phospholipid tails.[22] Considering that all of the molecules within this study interacted with the headgroups of AOT and the phospholipids, it is feasible that at least some of these molecules may affect the phospholipid tails as well. If these molecules affect the phospholipid tails then such interaction might aid in the crossing of the drugs across the phospholipid bilayer. Additional studies are needed to determine if these small molecules passively diffuse across bilayers, but these studies provide the framework to build a more in depth understanding of small molecule interactions with membrane interfaces.

CONCLUSIONS

We found that the interactions of INH, BHZ, BA, PIC, NIC, and iNIC, all interact with phospholipid and surfactant interfaces with the phospholipid/surfactant head groups, but have different effects on phospholipid interfaces. The phospholipid Langmuir monolayer studies show a difference in interaction of the small molecules that were not only dependent on the structure of the small molecules but also the phospholipids themselves. All the molecules tested reside within the water AOT surfactant interface of RMs with the amide/

hydrazide facing toward the water pool except of NIC and PIC. NIC and PIC resided at the interface but were tilted with the amide of NIC facing more away from the water pool than the amide of PIC. In summary, we show here that interactions of small aromatic N-containing molecules with lipid surfactant interfaces are not straight forward and that structural changes of the small aromatic compounds can alter their affinity for different phospholipid interfaces, how they affect different phospholipid interfaces, and the specifics behind the interactions with these interfaces.

Supplementary Material

Refer to Web version on PubMed Central for supplementary material.

ACKNOWLEDGMENTS

We thank Dr. Christopher D. Rithner for assistance with the NMR studies. D. C. Crans and D. C. Crick thank NIH for funding for this research (Grant # AI119567).

ABBREVIATIONS

AOT	aerosol-OT
RM	Reverse Micelle
DPPC	dipalmitoylphosphatidylcholine
DPPE	dipalmitoylphosphatidylethanolamine
DMPC	dimyristoylphosphatidylcholine
INH	isoniazid
BHZ	benzhydrazide
iNIC	isonicotinamide
NIC	nicotinamide
PIC	picolinamide
BA	benzamide
DLS	dynamic light scattering
NMR	nuclear magnetic resonance
Rh	hydrodynamic radius
PDI	polydispersity index
DSS	2,2-dimethyl-2-silapentane-5-sulfonate sodium salt
TMS	tetramethyl silane. ROESY, rotating-frame Overhauser spectroscopy
NOESY	nuclear Overhauser effect spectroscopy; DDI H_2O, double deionized water

REFERENCES

(1). Azuma K; Ouchi Y; Inoue S Vitamin K: Novel Molecular Mechanisms of Action and Its Roles in Osteoporosis. Geriatr Gerontol Int. 2014, 14 (1), 1–7.

(2). Lambert RJ; Stratford M Weak-Acid Preservatives: Modelling Microbial Inhibition and Response. J. Appl. Microbiol 1999, 86 (1), 157–164. [PubMed: 10030018]

(3). Ullah A; Orij R; Brul S; Smits GJ Quantitative Analysis of the Modes of Growth Inhibition by Weak Organic Acids in Saccharomyces Cerevisiae. Appl. Environ. Microbiol 2012, 78 (23), 8377–8387. [PubMed: 23001666]

(4). Westfall DA; Krishnamoorthy G; Wolloscheck D; Sarkar R; Zgurskaya HI; Rybenkov VV Bifurcation Kinetics of Drug Uptake by Gram-Negative Bacteria. PLoS One. 2017, 12 (9), 1–18.

(5). Zhang Y; Wade MM; Scorpio A; Zhang H; Sun ZH Mode of Action of Pyrazinamide: Disruption of Mycobacterium Tuberculosis Membrane Transport and Energetics by Pyrazinoic Acid. J. Antimicrob. Chemother 2003, 52 (5), 790–795. [PubMed: 14563891]

(6). Bardou F; Raynaud C; Ramos C; Laneelle MA; Laneelle G Mechanism of Isoniazid Uptake in Mycobacterium Tuberculosis. Microbiology-Uk. 1998, 144, 2539–2544.

(7). Unissa AN; Subbian S; Hanna LE; Selvakumar N Overview on Mechanisms of Isoniazid Action and Resistance in Mycobacterium Tuberculosis. Infect., Genet. Evol 2016, 45, 474–492. [PubMed: 27612406]

(8). Finkelst A Weak-Acid Uncouplersof Oxidative Phosphorylation - Mechanism of Action on Thin Lipid Membranes. Biochim. Biophys. Acta 1970, 205 (1), 1–6. [PubMed: 5439517]

(9). Olsson A; Olofsson T; Pero RW Specific Binding and Uptake of Extracellular Nicotinamide in Human Leukemic K-562 Cells. Biochem. Pharmacol 1993, 45 (6), 1191–1200. [PubMed: 8466540]

(10). Piper P; Mahe Y; Thompson S; Pandjaitan R; Holyoak C; Egner R; Muhlbauer M; Coote P; Kuchler K The Pdr12 Abc Transporter Is Required for the Development of Weak Organic Acid Resistance in Yeast. EMBO J. 1998, 17 (15), 4257–4265. [PubMed: 9687494]

(11). Silve A; Mir LM Cell Electropermeabilization and Cellular Uptake of Small Molecules: The Electrochemotherapy Concept. 2011; p 69–82.

(12). Wilson DF; Ting HP; Koppelman MS Mechanism of Action of Uncouplers of Oxidative Phosphorylation. Biochemistry. 1971, 10 (15), 2897–2902. [PubMed: 5114533]

(13). Ivanova N; Ivanova A Testing the Limits of Model Membrane Simulationsbilayer Composition and Pressure Scaling. J. Comput. Chem 2018, 39 (8), 387–396. [PubMed: 29164634]

(14). Singer SJ; Nicolson GL The Fluid Mosaic Model of the Structure of Cell Membranes. Science. 1972, 175 (4023), 720–730. [PubMed: 4333397]

(15). van Meer G; Voelker DR; Feigenson GW Membrane Lipids: Where They Are and How They Behave. Nat. Rev. Mol. Cell Biol 2008, 9 (2), 112–124. [PubMed: 18216768]

(16). Alvarez R; Aramburu L; Puebla P; Caballero E; Gonzalez M; Vicente A; Medarde M; Pelaez R Pyridine Based Antitumour Compounds Acting at the Colchicine Site. Curr. Med. Chem 2016, 23 (11), 1100–1130. [PubMed: 27117490]

(17). Nayyar A; Jain R Recent Advances in New Structural Classes of Anti-Tuberculosis Agents. Curr. Med. Chem 2005, 12 (16), 1873–1886. [PubMed: 16101507]

(18). Prachayasittikul S; Pingaew R; Worachartcheewan A; Sinthupoom N; Prachayasittikul V; Ruchirawat S; Prachayasittikul V Roles of Pyridine and Pyrimidine Derivatives as Privileged Scaffolds in Anticancer Agents. Mini-Rev. Med. Chem 2017, 17 (10), 869–901. [PubMed: 27670581]

(19). Borba A; Albrecht M; Gomez-Zavaglia A; Lapinski L; Nowak MJ; Suhm MA; Fausto R Dimer Formation in Nicotinamide and Picolinamide in the Gas and Condensed Phases Probed by Infrared Spectroscopy. PCCP. 2008, 10 (46), 7010–7021. [PubMed: 19030597]

(20). Borba A; Gomez-Zavaglia A; Fausto R Molecular Structure, Vibrational Spectra, Quantum Chemical Calculations and Photochemistry of Picolinamide and Isonicotinamide Isolated in Cryogenic Inert Matrixes and in the Neat Low-Temperature Solid Phases. J. Phys. Chem. A 2008, 112 (1), 45–57. [PubMed: 18069805]

(21). Martini MF; Disalvo EA; Pickholz M Nicotinamide and Picolinamide in Phospholipid Monolayers. Int. J. Quantum Chem 2012, 112 (20), 3289–3295.

(22). Borba A; Lairion F; Disalvo A; Fausto R Interaction of Nicotinamide and Picolinamide with Phosphatidylcholine and Phosphatidylethanolamine Membranes: A Combined Approach Using Dipole Potential Measurements and Quantum Chemical Calculations. Biochim. Biophys. Acta, Biomembr 2009,Z 1788 (12), 2553–2562.

(23). Gzyl-Macher B; Handzlik J; Nowak-Stpniowska A Interactions of Phenytoin with Lipids in Mixed Langmuir Monolayers. Colloids Surf., A 2008, 321 (1–3), 52–59.

(24). Gzyl-Malcher B; Handzlik J; Klekowska E Interaction of Prazosin with Model Membranes - a Langmuir Monolayer Study. Bioelectrochemistry. 2012, 87, 96–103. [PubMed: 22260980]

(25). Jurak M Thermodynamic Aspects of Cholesterol Effect on Properties of Phospholipid Monolayers: Langmuir and Langmuir-Blodgett Monolayer Study. J. Phys. Chem. B 2013, 117 (13), 3496–3502. [PubMed: 23470025]

(26). Hoyo J; Torrent-Burgues J; Guaus E Biomimetic Monolayer Films of Monogalactosyldiacylglycerol Incorporating Ubiquinone. J. Colloid Interface Sci 2012, 384, 189–197. [PubMed: 22835734]

(27). Nerdal W; Nilsen TRS; Steinkopf S Coenzyme Q(10), Localizations in Model Membranes. A Langmuir Monolayer Study. Biophys. Chem 2015, 207, 74–81. [PubMed: 26408828]

(28). Roche Y; Peretti P; Bernard S Influence of the Chain Length of Ubiquinones on Their Interaction with Dppc in Mixed Monolayers. Biochim. Biophys. Acta, Biomembr 2006, 1758 (4), 468–478.

(29). Choi Y; Attwood SJ; Hoopes MI; Drolle E; Karttunen M; Leonenko Z Melatonin Directly Interacts with Cholesterol and Alleviates Cholesterol Effects in Dipalmitoylphosphatidylcholine Monolayers. Soft Matter. 2014, 10 (1), 206–213. [PubMed: 24651707]

(30). Peters BJ; Groninger AS; Fontes FL; Crick DC; Crans DC Differences in Interactions of Benzoic Acid and Benzoate with Interfaces. Langmuir. 2016, 32 (37), 9451–9459. [PubMed: 27482911]

(31). Sostarecz AG; Gaidamauskas E; Distin S; Bonetti SJ; Levinger NE; Crans DC Correlation of Insulin-Enhancing Properties of Vanadium-Dipicolinate Complexes in Model Membrane Systems: Phospholipid Langmuir Monolayers and Aot Reverse Micelles. Chem. - Eur. J 2014, 20 (17), 5149–5159. [PubMed: 24615733]

(32). Chimote G; Banerjee R Effect of Antitubercular Drugs on Dipalmitoylphosphatidylcholine Monolayers: Implications for Drug Loaded Surfactants. Respir. Physiol. Neurobiol 2005, 145 (1), 65–77. [PubMed: 15652789]

(33). Kaganer VM; Mohwald H; Dutta P Structure and Phase Transitions in Langmuir Monolayers. Rev. Mod. Phys 1999, 71 (3), 779–819.

(34). Veldhuizen EJA; Haagsman HP Role of Pulmonary Surfactant Components in Surface Film Formation and Dynamics. Biochim. Biophys. Acta, Biomembr 2000, 1467 (2), 255–270.

(35). Veldhuizen R; Nag K; Orgeig S; Possmayer F The Role of Lipids in Pulmonary Surfactant. Biochim. Biophys. Acta, Mol. Basis Dis 1998, 1408 (2–3), 90–108. [PubMed: 9813256]

(36). Wustneck R; Perez-Gil J; Wustneck N; Cruz A; Fainerman VB; Pison U Interfacial Properties of Pulmonary Surfactant Layers. Adv. Colloid Interface Sci 2005, 117 (1–3), 33–58. [PubMed: 16120435]

(37). Nowotarska SW; Nowotarski KJ; Friedman M; Situ C Effect of Structure on the Interactions between Five Natural Antimicrobial Compounds and Phospholipids of Bacterial Cell Membrane on Model Monolayers. Molecules. 2014, 19 (6), 7497–7515. [PubMed: 24914896]

(38). Sohlenkamp C; Geiger O Bacterial Membrane Lipids: Diversity in Structures and Pathways. FEMS Microbiol. Rev 2016, 40 (1), 133–159. [PubMed: 25862689]

(39). De TK; Maitra A Solution Behavior of Aerosol Ot in Nonpolar-Solvents. Adv. Colloid Interface Sci 1995, 59, 95–193.

(40). Eicke HF; Rehak J Formation of Water-Oil-Microemulsions. Helv. Chim. Acta 1976, 59 (8), 2883–2891.

(41). Maitra A Determination of Size Parameters of Water Aerosol Ot Oil Reverse Micelles from Their Nuclear Magnetic-Resonance Data. J. Phys. Chem 1984, 88 (21), 5122–5125.

(42). Zulauf M; Eicke HF Inverted Micelles and Microemulsions in the Ternary-System H_2O-Aerosol-Ot-Isooctane as Studied by Photon Correlation Spectroscopy. J. Phys. Chem 1979, 83 (4), 480–486.

(43). Crans DC; Trujillo AM; Bonetti S; Rithner CD; Baruah B Levinger NE Penetration of Negatively Charged Lipid Interfaces by the Doubly Deprotonated Dipicolinate. J. Org. Chem 2008, 73 (24), 9633–9640. [PubMed: 19053583]

(44). Crans DC; Trujillo AM; Pharazyn PS; Cohen MD How Environment Affects Drug Activity: Localization, Compartmentalization and Reactions of a Vanadium Insulin Enhancing Compound, Dipicolinatooxovanadium(V). Coord. Chem. Rev 2011, 255 (19–20), 2178–2192.

(45). Koehn JT; Magallanes ES; Peters BJ; Beuning CN; Haase AA; Zhu MJ; Rithner CD; Crick DC; Crans DC A Synthetic Isoprenoid Lipoquinone, Menaquinone-2, Adopts a Folded Conformation in Solution and at a Model Membrane Interface. J. Org. Chem 2018, 83 (1), 275–288. [PubMed: 29168636]

(46). Samart N; Beuning CN; Haller KJ; Rithner CD; Crans D B Interaction of a Biguanide Compound with Membrane Model Interface Systems: Probing the Properties of Antimalaria and Antidiabetic Compounds. Langmuir. 2014, 30 (29), 8697–8706. [PubMed: 24956022]

(47). Sripradite J; Miller S; Tongraar A; Johnson M; Crans D Probing the Effects of Environments on Pka Values: Interaction of Aniline with Reverse Micelles as Monitored Using by 1h Nmr Spectroscopy. Abstr. Pap. Am. Chem. Soc 2015, 249.

(48). Leekumjorn S; Sum AK Molecular Simulation Study of Structural and Dynamic Properties of Mixed Dppc/Dppe Bilayers. Biophys. J 2006, 90 (11), 3951–3965. [PubMed: 16533838]

(49). Leekumjorn S; Sum AK Molecular Investigation of the Interactions of Trehalose with Lipid Bilayers of Dppc, Dppe and Their Mixture. Mol. Simul 2006, 32 (3–4), 219–230.

(50). Wang ZN; Yang SH Effects of Fullerenes on Phospholipid Membranes: A Langmuir Monolayer Study. Chemphyschem. 2009, 10 (13), 2284–2289. [PubMed: 19603448]

(51). Jones MN, Micelles, Monolayers, and Biomembranes. New York : Wiley-Liss: New York, 1995.

(52). Crans DC; Peters BJ; Wu X; McLauchlan CC Does Anion Cation Organization in Na+-Containing X-Ray Crystal Structures Relate to Solution Interactions in Inhomogeneous Nanoscale Environments: Sodium-Decavanadate in Solid State Materials, Minerals, and Microemulsions. Coord. Chem. Rev 2017, 344, 115–130.

(53). Vermathen M; Stiles P; Bachofer SJ; Simonis U Investigations of Monofluoro-Substituted Benzoates at the Tetradecyltrimethylammonium Micellar Interface. Langmuir. 2002, 18 (4), 1030–1042.

(54). Crans DC; Rithner CD; Baruah B; Gourley BL; Levinger NE Molecular Probe Location in Reverse Micelles Determined by Nmr Dipolar Interactions. J. Am. Chem. Soc 2006, 128 (13), 4437–4445. [PubMed: 16569021]

(55). Crans DC; Levinger NE The Conundrum of Ph in Water Nanodroplets: Sensing Ph in Reverse Micelle Water Pools. Acc. Chem. Res 2012, 45 (10), 1637–1645. [PubMed: 22812536]

(56). Baruah B; Roden JM; Sedgwick M; Correa NM; Crans DC; Levinger NE When Is Water Not Water? Exploring Water Confined in Large Reverse Micelles Using a Highly Charged Inorganic Molecular Probe. J. Am. Chem. Soc 2006, 128 (39), 12758–12765. [PubMed: 17002370]

(57). Majumder R; Sarkar Y; Das S; Ray A; Parui PP Interfacial Ph and Polarity Detection of Amphiphilic Self-Assemblies Using a Single Schiff-Base Molecule. New J. Chem 2017, 41 (16), 8536–8545.

(58). Moran L; Scrimgeour K; Horton H; Ochs R; Rawn J, Biochemistry. 2 ed.; Neil Patterson: 1994.

(59). Perrin DD; International Union of P; Applied Chemistry. Commission on Electrochemical, D., Dissociation Constants of Organic Bases in Aqueous Solution. Butterworths: London :,1965.

(60). Marques AV; Trindade PM; Marques S; Brum T; Harte E; Rodrigues MO; D'Oca MGM; da Silva PA; Pohlmann AR; Alves ID; de Lima VR Isoniazid Interaction with Phosphatidylcholine-Based Membranes. J. Mol. Struct 2013, 1051, 237–243.

(61). Rodrigues C; Gameiro P; Prieto M; de Castro B Interaction of Rifampicin and Isoniazid with Large Unilamellar Liposomes: Spectroscopic Location Studies. Biochim. Biophys. Acta, Gen. Subj 2003, 1620 (1–3), 151–159. [PubMed: 12595084]

(62). Tollin G; Salamon Z; Hruby VJ Techniques: Plasmon-Waveguide Resonance (Pwr) Spectroscopy as a Tool to Study Ligand-Gpcr Interactions. Trends Pharmacol. Sci 2003, 24 (12), 655–659. [PubMed: 14654307]

(63). Contreras FX; Sanchez-Magraner L; Alonso A; Goni FM Transbilayer (Flip-Flop) Lipid Motion and Lipid Scrambling in Membranes. FEBS Lett. 2010, 584 (9), 1779–1786. [PubMed: 20043909]

(64). Gurtovenko AA; Vattulainen I Molecular Mechanism for Lipid Flip-Flops. J. Phys. Chem. B 2007, 111 (48), 13554–13559. [PubMed: 17988118]

(65). Henseleit U; Plasa G; Haest C Effects of Divalent-Cations on Lipid Flip-Flop in the Human Erythrocyte-Membrane. Biochim. Biophys. Acta 1990,1029 (1), 127–135. [PubMed: 2223803]

(66). Kandasamy SK; Larson RG Cation and Anion Transport through Hydrophilic Pores in Lipid Bilayers. J. Chem. Phys 2006,125 (7), 07491.

(67). Smeets EF; Comfurius P; Bevers EM; Zwaal RFA Calcium-Induced Transbilayer Scrambling of Fluorescent Phospholipid Analogs in Platelets and Erythrocytes. Biochim. Biophys. Acta, Biomembr 1994, 1195 (2), 281–286.

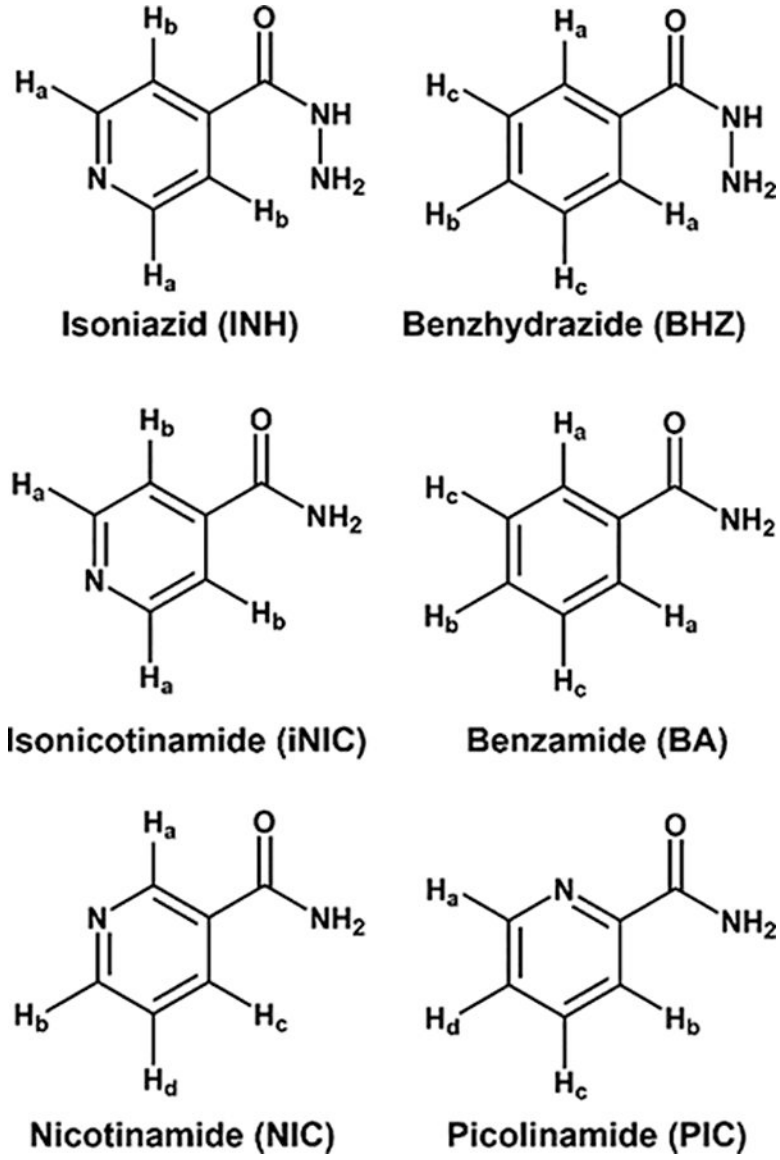

Figure 1.

Structures of isoniazid (INH), benzhydrazide (BHZ), isonicotinamide (iNIC), benzamide (BA), nicotinamide (NIC), and picolinamide (PIC), with protons labeled for ^{1}H NMR peak labeling. The protons in the ^{1}H NMR spectra has H_a as the most downfield ^{1}H NMR peak, Hb the next one, *etc.* See Figure S1 for enlargement.

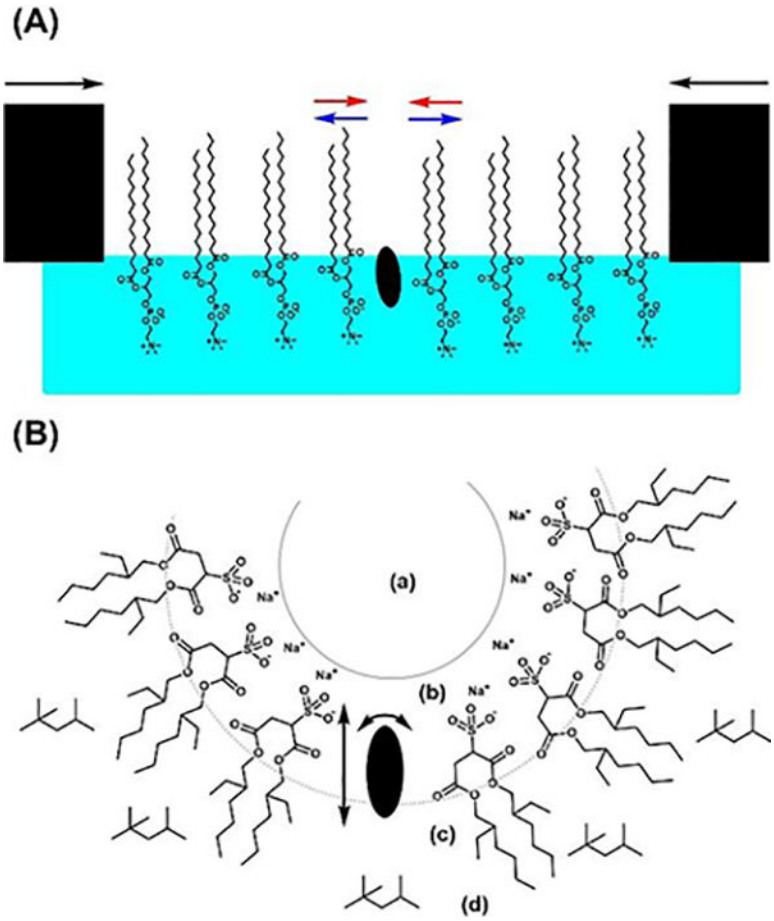

Figure 2.

The Langmuir monolayer (A) shows how a molecule can affect a phospholipid interface by penetrating and condensing (red arrows) or spreading (blue arrows) the phospholipids during a compression isotherm. The schematic depiction of a RM (B) outlines the area in which a molecule may reside, such as the bulk water (a), interfacial Stern layer (b), AOT tail region (c), and isooctane (d). The black oval demonstrates how a molecule can have varying depths within the RM interface along with different orientations. Figure adapted from Peters *et al.*[30]

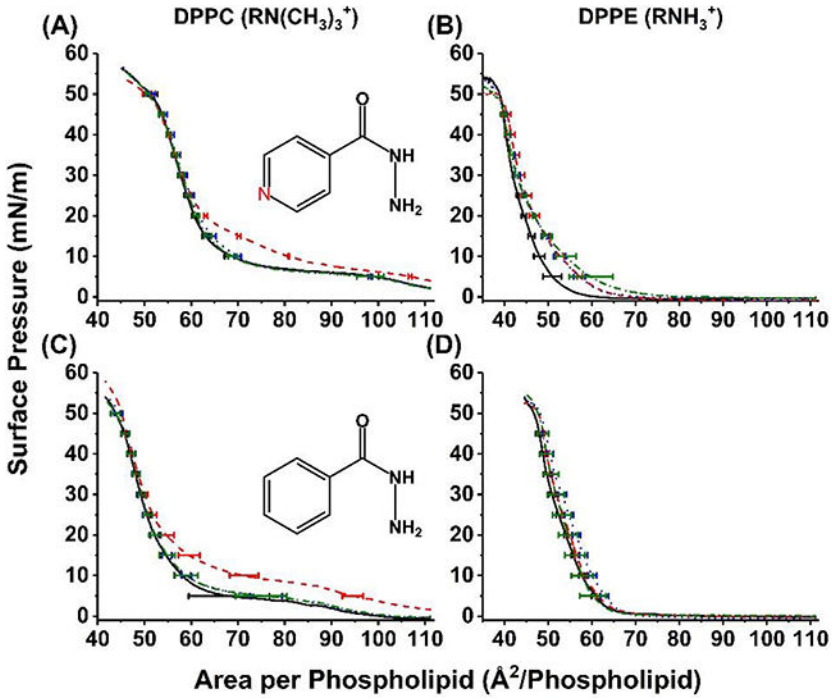

Figure 3.

Compression isotherms of DPPC (left column) or DPPE (right column) in the presence of INH (A and B) or BHZ (C and D). The solid black curves correspond to the control films without any hydrazide present. The other curves correspond to 10mM hydrazide (red dashed line), 1 mM (blue dotted line), and 0.1 mM (green dashed and dotted line) present in the 20 mM sodium phosphate buffered subphase (pH 7.4). Each curve is an average of at least 3 trials with standard deviations. The R group for each phospholipid includes the phosphate, glycerol, and fully saturated C_{16} tails. See Figures S4 and S5 for enlarged versions.

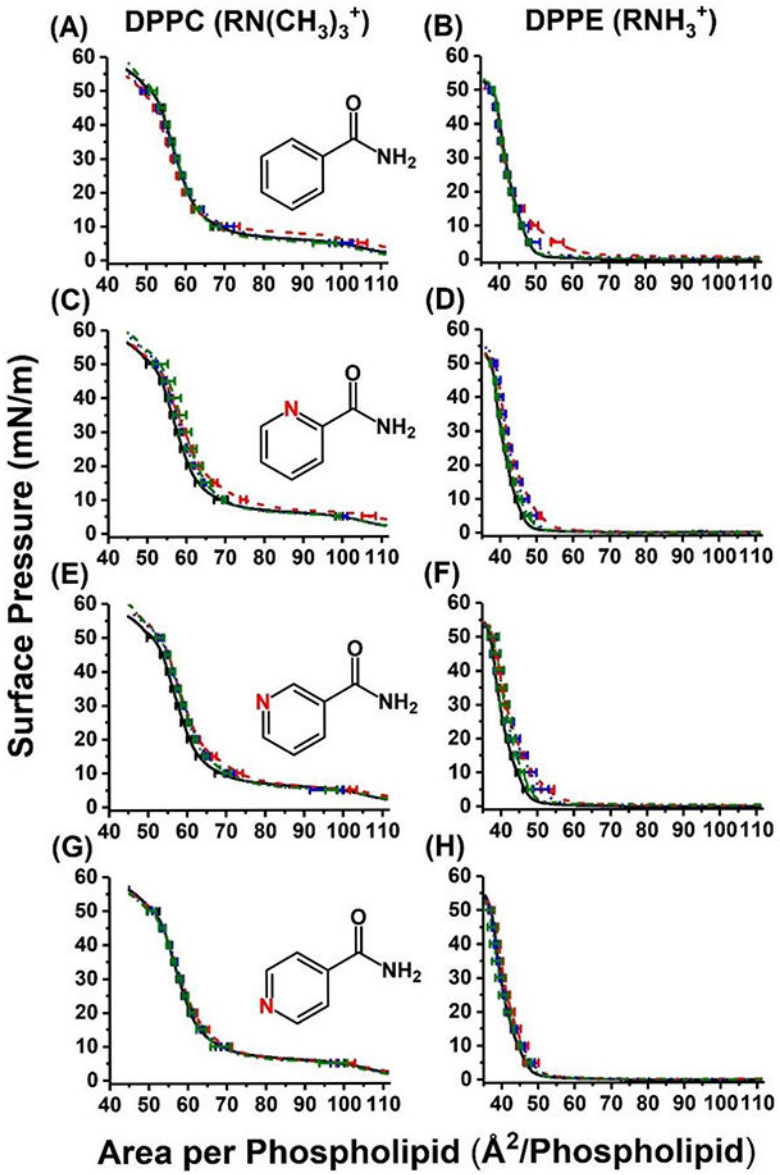

Figure 4:

The resulting surface pressure compression isotherms of DPPC (left column) and DPPE (right column) in the presence of BA (A and B), PIC, (C and D), NIC (E and F), iNIC (G and H) at concentrations of 0 mM (black solid line), 0.1 mM (green dashed and dotted line), 1.0 mM (blue dotted line), and 10 mM (red dashed line) in the 20 mM sodium phosphate buffered subphase (pH 7.4). Each curve is an average of at least 3 trials with standard deviations. The R group for each phospholipid includes the phosphate, glycerol, and fully saturated Ci6 tails. See Figures S7-S10 for enlarged versions.

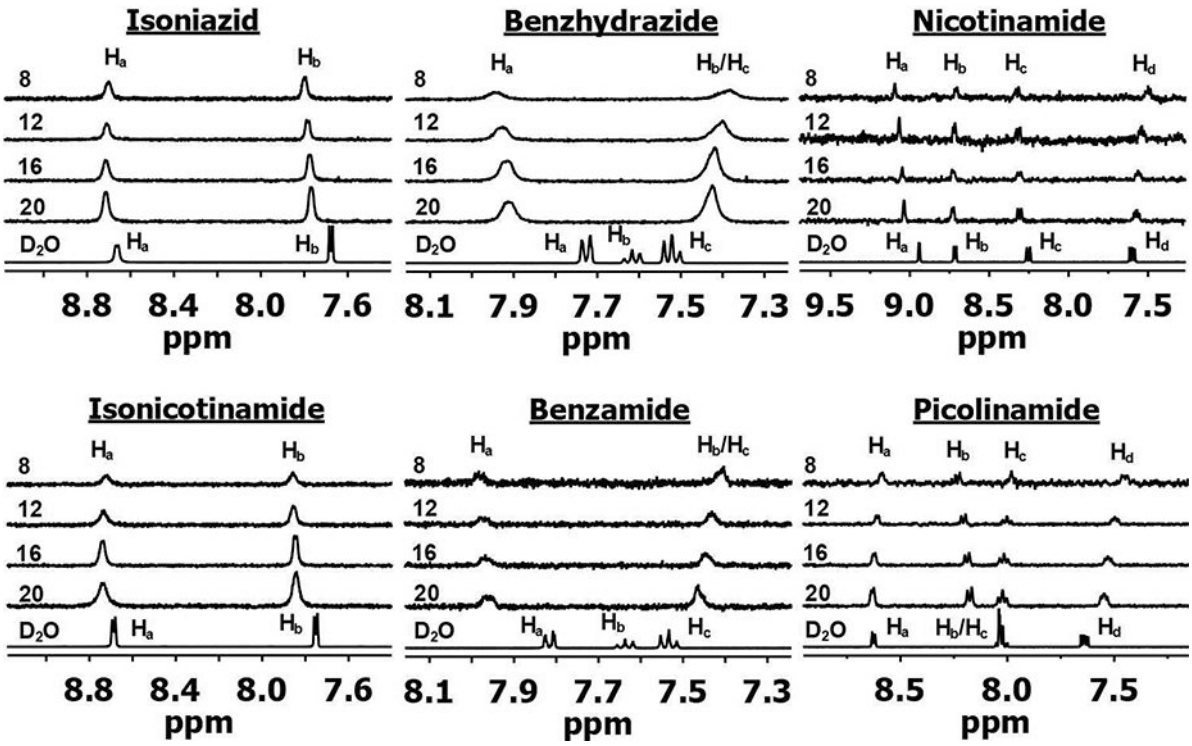

Figure 5.

1D ^{1}H NMR spectra obtained using a 400 MHz Varian NMR of INH, iNIC, BHZ, BA, NIC, and PIC in D_2O and varying sizes of RMs (w_0) given on the left of each stack of spectra. See Figure 1 for labeled structures corresponding to peak labels.

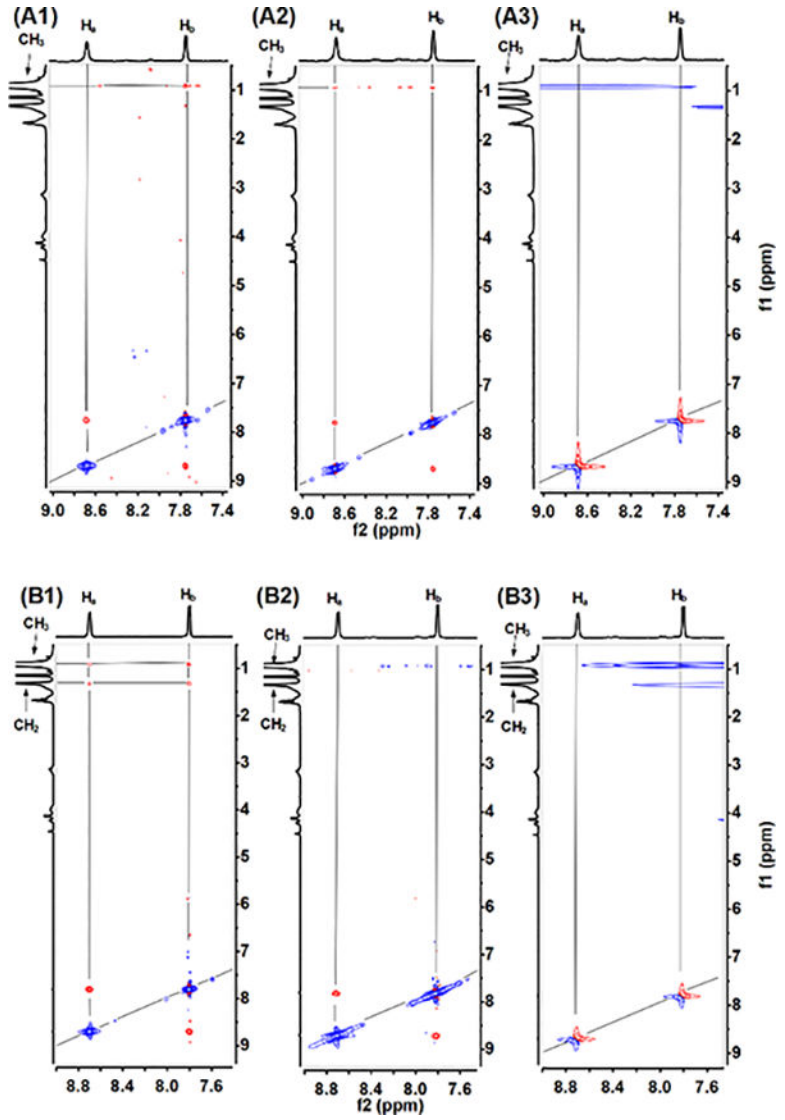

Figure 6:

^{1}H-^{1}H 2D ROESY NMR spectra acquired using a 400 MHz Inova NMR of INH (A1-A3) and iNIC (B1-B3) using 200 ms, 100 ms, and 0 ms mixing time (1–3) and a relaxation delay of 1.5 s. The diagonal is indicated by the diagonal line. The lines also highlight any off diagonal cross peaks.

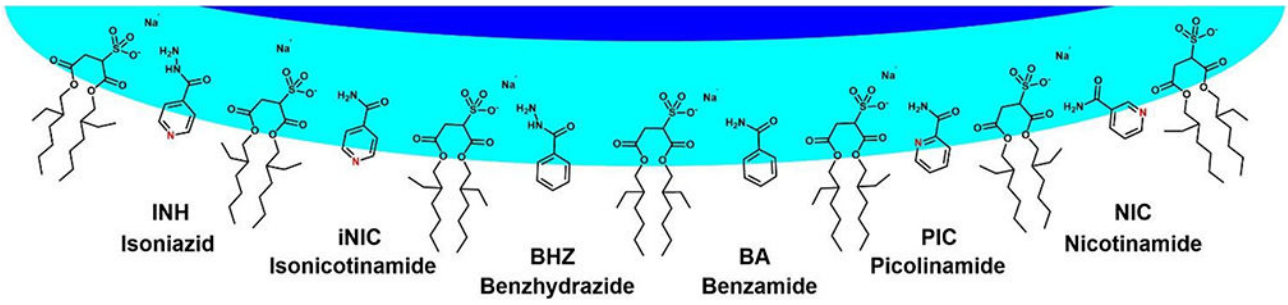

Figure 7:

Pictorial representation of the placement of INH, iNIC, BHZ, BA, PIC, and NIC within the RM as determined through ID and 2D ^{1}H NMR studies. It is important to note that this system is highly dynamic and therefore these are average positions/orientation within the AOT interface based on the ID and 2D NMR data presented in this study.

Table 1.

Percent Difference of Monolayer Surface Area in the Presence of Aromatic N-Substituted Compounds.[a]

N-substituted	Surface Pressure (mN/m)	DPPC	DPPE
		% difference from control	% difference from control
INH	5	7.36	12.25
	30	0.89	3.61
	35	0.10	3.22
BHZ	5	38.84	1.06
	30	1.86	2.02
	35	1.14	1.95
BA	5	6.21	16.19
	30	−2.20*	−0.92
	35	−2.19*	1.46
PIC	5	2.41	7.65
	30	3.32*	3.65**
	35	2.47**	3.44**
NIC	5	3.42	13.33
	30	3.01**	4.08**
	35	2.77**	3.62**
iNIC	5	1.22	3.32
	30	1.03	1.87
	35	0.55	1.89

[a]Surface pressures were chosen based on initial curve (5 mN/m) and physiological relevance (30–35 mN/m).[51] Significance of the percent difference was determined using a Student's T test with

*$p < 0.10$ and

**$p < 0.05$.

Table 2.

pk_a, Values of the Hydrazides and Amides of Interest in Aqueous and RM Solutions

Compound	Predicted pK_a	Reported pK_a[59]	pK_a in D_2O	pK_a in w_0 16 RM
INH	3.4, 2.4 *	3.5, 1.9 *	3.3	<1
BZH	2.8 *	3.0 *	2.8 *	<1
BA	−0.36	N.A.	N.A.	N.A.
PIC	2.2	2.1	2.4	<1
NIC	3.6	3.3	3.7	<1
iNIC	3.5	3.6	3.9	<1

* The table above outlines the pk_a, values determined using the method outlined in Figure S3. The $pK_a$of the amine protons for INH and BZH are given by.

The predicted pK_a values are from http://www.chemicalize.org. The reported pK_a values are from ref 59.[59]